

Phosphorylated Cellulose Nanofibrils: A Renewable Nanomaterial for the Preparation of Intrinsically Flame-Retardant Materials

*Original*

Phosphorylated Cellulose Nanofibrils: A Renewable Nanomaterial for the Preparation of Intrinsically Flame-Retardant Materials / Ghanadpour, Maryam; Carosio, Federico; Larsson, Per Tomas; Wågberg, Lars. - In: BIOMACROMOLECULES. - ISSN 1525-7797. - 16:10(2015), pp. 3399-3410. [10.1021/acs.biomac.5b01117]

*Availability:*

This version is available at: 11583/2655823 since: 2016-11-15T07:26:06Z

*Publisher:*

American Chemical Society

*Published*

DOI:10.1021/acs.biomac.5b01117

*Terms of use:*

This article is made available under terms and conditions as specified in the corresponding bibliographic description in the repository

*Publisher copyright*

GENERIC -- per es. Nature : semplice rinvio dal preprint/submitted, o postprint/AAM [ex default]

The original publication is available at <http://pubs.acs.org/journal/bomaf6> / <http://dx.doi.org/10.1021/acs.biomac.5b01117>.

(Article begins on next page)

# Phosphorylated cellulose nanofibrils: A renewable nanomaterial for the preparation of intrinsically flame-retardant materials

Maryam Ghanadpour <sup>†,\*</sup>, Federico Carosio<sup>‡</sup>, Per Tomas Larsson <sup>§,§</sup> and Lars Wågberg <sup>†,§,\*</sup>

<sup>†</sup> Department of Fiber and Polymer Technology, KTH Royal Institute of Technology, SE-100 44 Stockholm, Sweden

<sup>‡</sup> Dipartimento di Scienza Applicata e Tecnologia, Politecnico di Torino, sede di Alessandria, Viale Teresa Michel 5, 15121 Alessandria, Italy

<sup>§</sup> Wallenberg Wood Science Center at the Department of Fiber and Polymer Technology, KTH Royal Institute of Technology, SE-100 44 Stockholm, Sweden

<sup>§</sup> Innventia AB, Drottning Kristinas Väg 61, SE-114 86, Stockholm, Sweden

## Abstract

Cellulose from wood fibers, can be modified for use in flame retardant composites as an alternative to halogen-based compounds. For this purpose, sulfite dissolving pulp fibers have been chemically modified by phosphorylation and the resulting material has been used to prepare cellulose nanofibrils (CNF) having a width of approximately 3 nm. The phosphorylation was achieved using  $(\text{NH}_4)_2\text{HPO}_4$  in the presence of urea, and the degree of substitution (DS) by phosphorus was determined by X-Ray Photoelectron Spectroscopy (XPS), Conductometric titration and Nuclear Magnetic Resonance (NMR) spectroscopy. The presence of phosphate

groups in the structure of CNF has been found to noticeably improve the flame retardancy of this material. The nanopaper sheets prepared from phosphorylated CNF showed self-extinguishing properties after consecutive applications of a methane flame for 3s and did not ignite under a heat flux of  $35\text{kW/m}^2$ , as shown by flammability and cone calorimetry measurements, respectively.

**Keywords:** Cellulose nanofibrils, Flame-retardancy, Morphology, Phosphorylation

## 1. Introduction

During recent decades the extensive use of polymeric materials in fields such as transport, military and furniture upholstery has led to extensive scientific activities to overcome the tendency of this class of materials to easily decompose and ignite when heated. This has made it necessary to blend flame-retardants into the used polymers<sup>1,2</sup>. Flame-retardants may be based on halogens, phosphorus, nitrogen, metal ions or nanofillers<sup>3</sup>. The halogen-based compounds, which are the most effective and cost-efficient flame-retardant additives, have been criticized for both environmental and functional reasons. They can be leached from the polymer into the environment and can accumulate inside human and animal bodies. Moreover, during combustion they release toxic gases<sup>2,4</sup>. Phosphorus-containing flame retardants are more suitable than halogen-based compounds. Phosphorus-based compounds favor the formation of char instead of combustible volatile species<sup>5</sup>. The char, a multi-lamellar carbonaceous structure, acts as a thermal insulator and protects the surrounded polymer from further decomposition and thus has a flame-retardant effect<sup>6,7</sup>. Phosphorus chemistry is usually stated to represent the new frontier in the development of flame-retardant materials.

The use of phosphorus chemistry in combination with biomacromolecules is of great interest as it would give access to renewable resources characterized by intrinsic flame-retardant properties.

1 Cellulose nanofibrils (CNF) are one of the most interesting biomaterials for this task. The unique  
2 properties of CNF, including excellent mechanical properties, high specific surface area and high  
3 length-to-diameter ratio<sup>8</sup>, have made it suitable for the preparation of multifunctional materials  
4 such as thin films<sup>9</sup>, nanopaper<sup>10</sup>, foams and aerogels<sup>11,12</sup>. Imparting flame retardancy to cellulose  
5 fibrils will make these materials more feasible and safe for industrial applications.

6 Nanofibrils were first extracted from wood fibers by Turbak et al. in the early 1980s using  
7 repeated mechanical treatment with a high-pressure homogenizer to produce cellulose micro  
8 fibrils<sup>13</sup> with a width between 25 and 100 nm<sup>14</sup>. But, due to the high cost of production and lack  
9 of successful applications, these materials were not developed further. More recently it has been  
10 shown that different pretreatments of delignified wood fibers including combinations of  
11 enzymatic, mechanical and chemical modifications lead to a more energy-efficient production of  
12 CNF by facilitating the homogenization process<sup>15,16</sup>. The introduction of charged groups onto  
13 pulp fibers through chemical modification is one way to enhance delamination of fiber walls by  
14 increasing the osmotic pressure inside the fiber wall and hence their swelling<sup>17</sup>. This can facilitate  
15 the disintegration of nanofibrils from the fiber wall, leading to less clogging and a lower energy  
16 consumption during the homogenization process<sup>14,18</sup>. Examples of such chemical pretreatments  
17 are the partial carboxymethylation of cellulose<sup>19</sup> or the use of TEMPO (2,2,6,6-  
18 tertramethylpiperidine-1-oxyl)-mediated oxidation of cellulose, a regioselective reaction which  
19 introduces carboxylate groups to primary hydroxyl groups at the C6 position of the cellulose  
20 molecules<sup>15</sup>.

21 In this work, we propose a pretreatment of pulp fibers by phosphorylation which can facilitate the  
22 preparation of CNF by pre-charging the fiber wall through the introduction of anionic phosphate

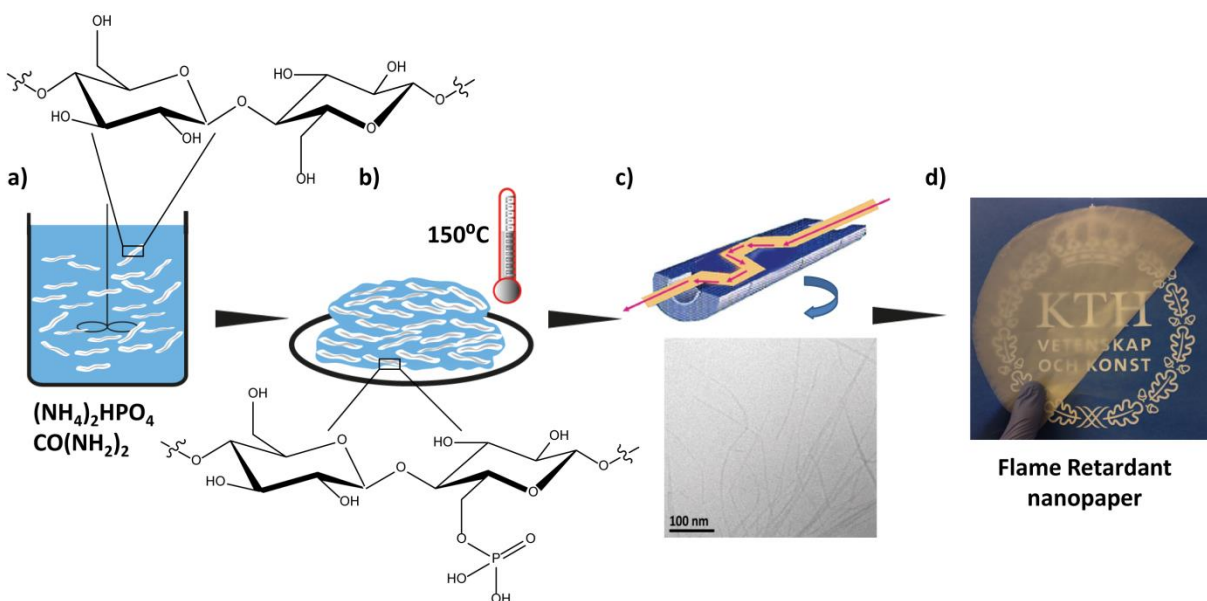


**Figure 1.** Schematic description of different steps for preparation of nanopaper sheet from phosphorylated CNF used in the present work: (a) Impregnation of fibers in a water solution of  $(\text{NH}_4)_2\text{HPO}_4$  and urea; (b) curing of fibers; (c) Top, basic design of an interaction chamber of a homogenizer where fibers disintegrate to fibrils<sup>14</sup> and bottom, TEM image of phosphorylated CNF; (d) Flame-retardant nanopaper sheet prepared in the Rapid –Köthen instrument (The KTH logo is used with permission from KTH Royal Institute of Technology)

groups and also contribute to the thermal stability and flame-retardant properties of the resulting material. Phosphorylation of cellulosic materials using phosphorylating agents such as phosphorus oxychloride ( $\text{POCl}_3$ ), phosphorus pentoxide ( $\text{P}_2\text{O}_5$ )<sup>20,21</sup>, phosphoric acid ( $\text{H}_3\text{PO}_4$ )<sup>22–24</sup>, di-ammonium hydrogen phosphate  $(\text{NH}_4)_2\text{HPO}_4$ <sup>25</sup> and organophosphates<sup>26</sup> has been studied for decades. It has been shown that the degree of substitution (DS) by phosphorus depends on the molar ratio of the phosphorylating agent and anhydroglucose units of cellulose and the time and temperature of the reaction<sup>20,21,23,27</sup>. Phosphorylation usually takes place in the presence of an organic solvent such as N,N-dimethylformamide (DMF), pyridine<sup>20,26</sup> or urea<sup>22–25,27</sup> which has a swelling effect on the cellulose-rich fibers and is a medium for phosphorylation reaction<sup>25</sup>.

Although extensive research has been devoted to the phosphorylation of cellulose, this approach has, to the author's knowledge, never been used for the production of intrinsically flame-retardant CNF. In order to benefit from less toxic chemicals, an ammonium salt of phosphoric acid ((NH<sub>4</sub>)<sub>2</sub>HPO<sub>4</sub>) is used as the phosphorylating agent and this leads to less cellulose hydrolysis than phosphoric acid. Figure 1 shows a diagram of the phosphorylation procedure followed by preparation of phosphorylated CNF and the flame-retardant nanopaper sheet. The phosphorylation process has been characterized by Attenuated Total Reflection Fourier Transform Infrared (ATR-FTIR) spectroscopy, X-Ray Photoelectron Spectroscopy (XPS) and Nuclear Magnetic Resonance (NMR) spectroscopy. In addition to its chemical composition, the phosphorylated CNF has been characterized regarding the dimensions and extent of fibrillation, using cryo-TEM and Atomic Force Microscopy. Finally, the phosphorylated CNF has been used to prepare nanopaper sheets that have been characterized with respect to their mechanical and flame retardancy properties.

## Experimental

**2.1. Materials.** *2.1.1. Chemicals.* Di-Ammonium hydrogen phosphate (ACS reagent grade) was purchased from Merck Millipore, and urea (ReagentPlus ≥ 99.5%) was provided by Sigma Aldrich. Deionized water was used in all reactions. Sodium bicarbonate, hydrochloric acid and sodium hydroxide were all of analytical grade and supplied by Merck KGaA.

*2.1.2. Fibers.* A commercial sulfite softwood dissolving pulp (Domsjö Dissolving plus; Domsjö Fabriker AB, Domsjö, Sweden) from 60% Norwegian spruce and 40% Scots pine, with a hemicellulose content of 4.5% and a lignin content of 0.6% was supplied in a dried form.

**2.2. Methods.** *2.2.1. Preparation of fibers.* Prior to chemical modification, fibers were re-slushed and washed in deionized water, after which the carboxyl groups on the fibers were converted to their sodium form using a standard washing process described earlier<sup>19</sup>. Once washed, the fibers were refined in a PFI mill (HAM-JERN, Hamar, Norway) for 4000 rev. Thereafter a fiber dispersion of 5g/L was fractionated by continuous washing with approximately 10 liters of deionized water in a Britt Drainage Jar fitted with a 50 mesh metallic wire to remove the fines liberated during the refining.

*2.2.2. Phosphorylation.* Phosphorylation was carried out using  $(\text{NH}_4)_2\text{HPO}_4$  in the presence of urea. Assuming cellulose chains to be the main constituents of the pulp fibers (94.9%); two different molar ratios of anhydroglucose units (AGU) to reagents were used as shown in Table 1.

**Table 1.** Molar ratios and reaction times used for phosphorylation of fibers

Sample	Molar ratio	Time (min) / Temperature (°C)
	AGU:( $\text{NH}_4$ ) <sub>2</sub> HPO <sub>4</sub> :Urea	
L10	1: 1.2: 4.9	10 / 150
L30	1: 1.2: 4.9	30 / 150
L60	1: 1.2: 4.9	60 / 150
L90	1: 1.2: 4.9	90 / 150
H10	1: 2.5: 10	10 / 150
H30	1: 2.5: 10	30 / 150
H60	1: 2.5: 10	60 / 150
H90	1: 2.5: 10	90 / 150

Excess amounts of urea are usually used in phosphorylation reaction<sup>23,25,27</sup> to prevent degradation of cellulose due to the release of phosphoric acid during curing at elevated temperatures. In each case, approximately 4 moles of urea were therefore used per mole of  $(\text{NH}_4)_2\text{HPO}_4$ . The phosphorylation process consisted of impregnation and curing. During

1 impregnation, urea and  $(\text{NH}_4)_2\text{HPO}_4$  were added to a fiber dispersion of 1 wt.% in deionized  
2 water under continuous stirring. The aqueous solution was then filtered to a 10 wt.% fiber  
3 dispersion. The fibers were then dried in an oven at 70°C followed by curing at 150°C for 10, 30,  
4 60 or 90 minutes, denoted as L10/H10, L30/H30, L60/H60 and L90/H90 respectively. The  
5 phosphorylated fibers were then washed with 2 liters of boiling and 2 liters of cold deionized  
6 water to remove loosely attached chemicals.

7 *2.2.3. Preparation of phosphorylated CNF.* Phosphorylated CNF was prepared using a high  
8 pressure homogenization technique<sup>28</sup>. A 2 wt.% dispersion of L10, L30 or L60 was prepared in  
9 deionized water, and the pH of the dispersion was set to 9.5 using 1 M NaOH to ensure complete  
10 dissociation of carboxylate and phosphate groups. The fiber dispersion was then passed through a  
11 high pressure homogenizer (Microfluidizer M-110EH, Microfluidics Corp.) equipped with two  
12 chambers of different sizes connected in series (200 and 100  $\mu\text{m}$ ). Full homogenization was  
13 achieved with a single pass through the large chamber (200  $\mu\text{m}$ ) and six passes through the  
14 smaller chamber (100  $\mu\text{m}$ ).

15 *2.2.4. Preparation of nanopaper sheet.* Phosphorylated CNF produced from L10 was used to  
16 prepare nanopaper sheets based on the method described elsewhere<sup>10</sup>. The sheets were prepared  
17 using a semiautomatic sheet former (Rapid-Köthen, PTI, Vorchdorf, Austria) where the fibril  
18 dispersion is filtered through a membrane and the wet gel obtained is dried under vacuum<sup>10</sup>. A  
19 hydrophilic durapore membrane with a pore size of 0.45  $\mu\text{m}$  was used.

## 20 **2.3. Characterization Techniques.** *2.3.1. Total charge determination.* The total charge

21 density of the phosphorylated fibers was determined by conductometric titration where fibers in  
22 their proton form were titrated against NaOH. For this purpose, the fibers were dispersed in

1 deionized water at a fiber concentration of 0.5-1g/l. The pH and salt (NaCl) concentration of the  
2 fiber dispersion was adjusted to pH: 3.5 (using 0.01M HCL) and 2mM respectively. The total  
3 charge was then determined by titration with 0.1M NaOH<sup>28</sup>.

4 *2.3.2. Attenuated Total Reflection Fourier Transform Infrared (ATR-FTIR) spectroscopy.* ATR-  
5 FTIR was performed using a Perkin-Elmer Spectrum 2000 FT-IR equipped with a single  
6 reflection accessory unit having a diamond ATR crystal (Golden Gate) from Gaseby Specac Ltd.  
7 (Kent, England). The ATR spectra were recorded at room temperature in the range of 4000-600  
8 cm<sup>-1</sup> as the average of 16 scans and 4 cm<sup>-1</sup> resolution.

9 *2.3.3. X-Ray Photoelectron Spectroscopy (XPS).* The XPS spectra were collected with a Kratos  
10 Axis Ultra DLD electron spectrometer using a monochromatic Al K $\alpha$  X-ray source operated at  
11 150 W. An analyzer pass energy of 160 eV for acquiring wide spectra and a pass energy of 20 eV  
12 for individual photoelectron lines were used. Fiber samples for the analysis were gently hand-  
13 pressed using a clean Ni spatula into a special powder sample holder. The surface potential was  
14 stabilized by the charge neutralization system of the spectrometer. The binding energy (BE) scale  
15 was referenced to the C<sub>1s</sub> line of aliphatic carbon, set at 285.0 eV. The spectra were analyzed  
16 with the Kratos software.

17 *2.3.4. Nuclear Magnetic Resonance (NMR) spectroscopy.* All samples were wetted with  
18 deionized water to a water content of 40–60% and packed uniformly in a zirconium oxide rotor.  
19 Recording spectra of wet rather than dry samples gives a higher apparent resolution<sup>29</sup>. The  
20 CP/MAS <sup>13</sup>C-NMR spectra were recorded in a Bruker Avance III AQS 400 SB instrument  
21 operating at 9.4 T. All measurements were made at 295 ( $\pm$ 1) K with a MAS rate of 10 kHz. A 4-  
22 mm double air-bearing probe was used. Acquisition was performed using a CP pulse sequence,

1 i.e., a 2.95 micro-seconds proton 90° pulse and a 800 microseconds ramped (100–50%) falling  
2 contact pulse, with a 2.5 seconds delay between repetitions. A SPINAL64 pulse sequence was  
3 used for <sup>1</sup>H decoupling. The Hartmann-Hahn matching procedure was based on glycine. The  
4 chemical shift scale was calibrated to the TMS ((CH<sub>3</sub>)<sub>4</sub>Si) scale by assigning the data point of  
5 maximum intensity in the α-glycine carbonyl signal to a shift of 176.03 ppm. A total of 4096 or  
6 16384 transients were recorded for each sample, giving an acquisition time of approximately 3 h  
7 or 12 h. The software for spectral fitting was developed at Innventia AB, Stockholm, Sweden and  
8 is based on a Levenberg-Marquardt algorithm<sup>30</sup>. All computations are based on integrated signal  
9 intensities obtained from the spectral fitting<sup>31</sup>. Cellulose I specific surface area was calculated  
10 from the lateral fibril aggregate dimensions by assigning a density of 1500 kg/m<sup>3</sup> to cellulose I<sup>32</sup>.

11 *2.3.5. Atomic Force Microscopy (AFM).* CNF fibrils were adsorbed from a 1g/L aqueous  
12 dispersion onto silicon wafers (Si-Mat Silicon Material, Germany) with an anchoring polymeric  
13 surface layer (25 kD polyethylenimine, Sigma Aldrich). The adsorption time was 5min followed  
14 by rinsing with Milli-Q water (18.2 MΩ). A Bruker multimode 8 AFM (Bruker Ltd. Germany)  
15 with Bruker ScanAsyst-air tips was used for imaging in the ScanAsyst mode. DIPimage software  
16 (Delft University of Technology, The Netherlands) was used to determine the width of fibrils  
17 based on the image intensities.

18 *2.3.6. Cryo-Transmission Electron Microscopy (cryo-TEM).* An electron microscope (cryo-TEM,  
19 CM120 Philips, The Netherlands) equipped with a post-column energy filter (Gatan GIF100) was  
20 used. A cryoholder (CT-300 Oxford Instruments, U.K.) and its work-station were used to transfer  
21 the specimen to the electron microscope. The acceleration voltage was 120kV and the images  
22 were recorded digitally with a CCD camera under low electron dose conditions. Samples were  
23 prepared in a controlled environment vitrification system, and 3μL of the sample was deposited

on lacey carbon-sputtered copper grids and plunged into liquid ethane ( $-180^{\circ}\text{C}$ ), and stored under liquid nitrogen until measurement. In order to determine the width of fibrils from TEM images, ImageJ (National Institute of Mental Health, Maryland, USA) software was used.

*2.3.7. Thermogravimetric analysis (TGA).* The thermal and thermo-oxidative stabilities of the filter paper and nanopaper sheet were evaluated in nitrogen and in air respectively, from 50 to  $800^{\circ}\text{C}$  with a heating rate of  $10^{\circ}\text{C}/\text{min}$  using a TAQ500 (Laboratory for Emerging Material and Technology, South Carolina, USA) The samples (approx. 10mg) were placed in open alumina pans in an inert or oxidative atmosphere (gas flow: 60ml/min).  $T_{\text{onset}10\%}$  (temperature at 10% of weight loss),  $T_{\text{max}}$  (temperature at maximum rate of weight loss) and the residue at  $800^{\circ}\text{C}$  were obtained from the measurements.

*2.3.8. Flammability.* Flammability tests were carried out in a horizontal configuration applying a methane flame for 3 s on the short side of the paper sheet samples (25x100 mm). The experiments were repeated three times for each material on separate samples. Parameters such as burning rate and final residual amount were evaluated.

*2.3.9. Cone Calorimetry.* The combustion of square paper sheets (filter and nanopaper sheet,  $100\times 100\text{ mm}^2$ ) was investigated by cone calorimetry (Fire Testing technology, FTT, West Sussex, UK) according to the ISO 5660 Standard. The samples were placed in a sample holder, and an irradiative heat flow of  $35\text{ kW}/\text{m}^2$  was used in a horizontal configuration following the procedure developed for thin samples described elsewhere<sup>33</sup>. Parameters such as Time to Ignition (TTI, s), Peak of Heat Release Rate (PHRR,  $\text{kW}/\text{m}^2$ ), Total Heat Release (THR,  $\text{MJ}/\text{m}^2$ ) and the final residual amount were evaluated. Three independent samples were tested for each material.

2.3.10. *Mechanical test.* Tensile stress/strain at break and Young's modulus of nanopaper sheets were evaluated using the Instron 5944 (Instron, High Wycombe, UK) instrument equipped with a 500N load cell. Specimens 40 mm in length, 60-70  $\mu\text{m}$  thick and 5 mm wide were tested at a strain rate of 2 mm/min.

All the samples were conditioned at  $23\pm 1$   $^{\circ}\text{C}$  and 50% R.H for at least 48 hr. prior to the mechanical, flammability and combustion tests.

## 2. Results

### 3.1. Chemical characterization of phosphorylated fibers. 3.1.1. Determination of the total

*charge of the fibers.* Figure 2 shows the change in total charge ( $\mu\text{eq/g}$ ) of the fibers measured by conductometric titration as a function of curing time for phosphorylated fibers. For the fibers, phosphorylated at a low molar ratio of  $\text{AGU}:(\text{NH}_4)_2\text{HPO}_4$ , the total charge increased up to 60 minutes curing followed by a slight decrease at longer curing times. With a higher molar ratio of  $\text{AGU}:(\text{NH}_4)_2\text{HPO}_4$  a maximum charge was achieved already after 30 minutes curing followed by a large decrease with longer curing times, i.e. H60 and H90. The decrease in the total charge at longer curing times may indicate cellulose dissolution following the phosphorylation reaction. This is consistent with the 0.3% and 2.6% mass loss for H60 and H90 respectively after the reaction, whereas a mass gain of 9.4% and 5.5% was observed for H10 and H30, probably due to grafting of phosphate groups onto the cellulose.

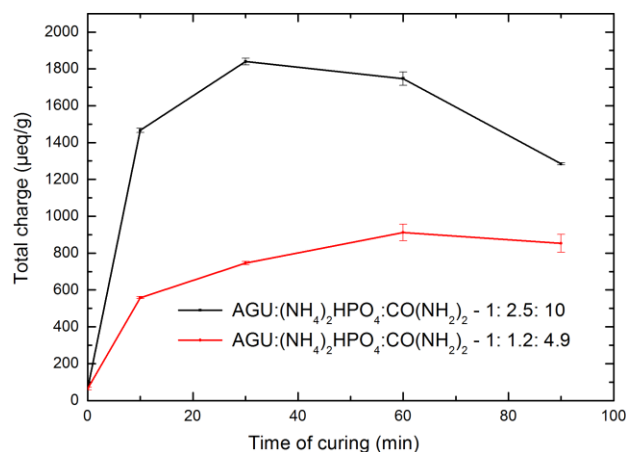


**Figure 2.** Total charge ( $\mu\text{eq/g}$ ) of phosphorylated fibers as a function of curing time: red line: AGU:( $\text{NH}_4$ ) $_2$ HPO $_4$ :Urea molar ratio of 1:1.2:4.9; black line: AGU:( $\text{NH}_4$ ) $_2$ HPO $_4$ :Urea molar ratio of 1:2.5:10

*3.1.2. ATR-FTIR spectroscopy analysis.* Figure 3 shows FTIR spectra of unmodified and phosphorylated fibers (3a for fibers modified at a low molar ratio of AGU:( $\text{NH}_4$ ) $_2$ HPO $_4$  and 3b at a high molar ratio case). Within the selected region, IR spectra of unmodified fibers show characteristic bands of cellulose chains including bands at 1165 and 1120  $\text{cm}^{-1}$  for C-O-C groups from glycosidic units or from  $\beta$ -(1 $\rightarrow$ 4)-glycosidic bonds<sup>27</sup>. The appearance of a new band at 1710  $\text{cm}^{-1}$  corresponding to the C=O stretching mode<sup>26</sup> for all the phosphorylated fibers supports the hypothesis that oxidation occurs during the reaction. Also the greater intensity of this band for L60, L90, H60 and H90 than for fibers cured for shorter times shows that oxidation increases with time, as expected. The phosphorylation is also supported by the appearance of a new band at 1230  $\text{cm}^{-1}$  corresponding to the P=O stretching mode<sup>24,27,34</sup> in all the phosphorylated samples. The appearance of new bands at 900-940  $\text{cm}^{-1}$  and 832  $\text{cm}^{-1}$  corresponding to the P-OH<sup>24,27</sup> stretching mode and the P-O-C aliphatic bond<sup>27</sup> respectively in the spectra of H10, H30, H60 and H90 also indicates the incorporation of phosphate groups and this increases slightly with the

curing time. In contrast these bands are not clearly observed in the case of fibers phosphorylated at the lower molar ratio of AGU:(NH<sub>4</sub>)<sub>2</sub>HPO<sub>4</sub>, probably because of the lower phosphorus content.

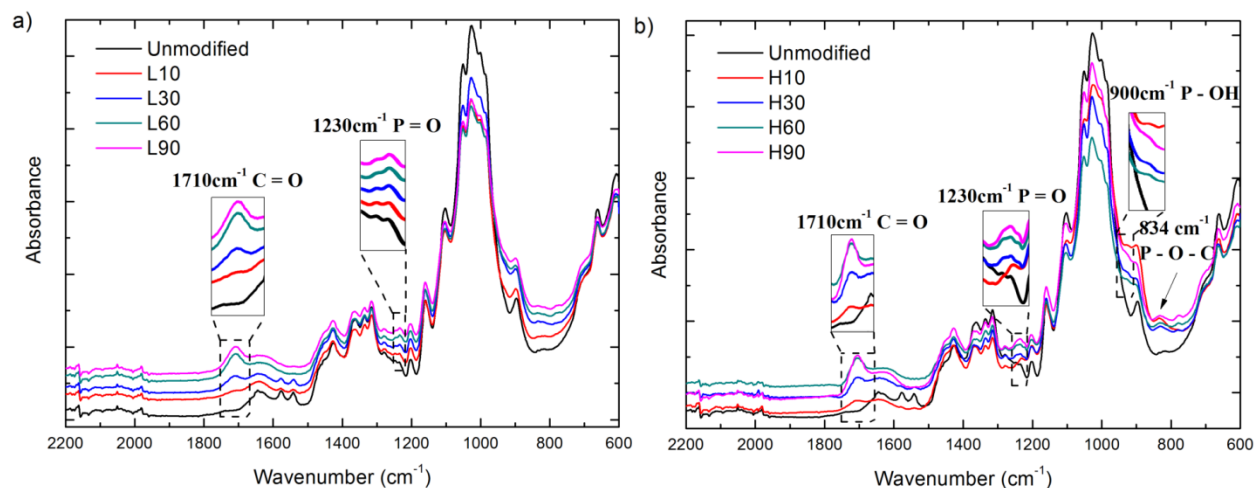


**Figure 3.** ATR-FTIR spectra of unmodified and phosphorylated fibers: (a) Fibers phosphorylated at a low molar ratio of AGU:(NH<sub>4</sub>)<sub>2</sub>HPO<sub>4</sub>; (b) Fibers phosphorylated at a high molar ratio of AGU:(NH<sub>4</sub>)<sub>2</sub>HPO<sub>4</sub>

**3.1.3. XPS analysis.** The XPS spectra of unmodified and phosphorylated fibers are shown in Figure 4 (4a showing XPS spectra of fibers modified at a low molar ratio of AGU:(NH<sub>4</sub>)<sub>2</sub>HPO<sub>4</sub> and 4b at a high molar ratio). Two distinct peaks of elemental C<sub>1s</sub> and O<sub>1s</sub> are present for unmodified fibers<sup>34–36</sup> as well as minor peaks which can be assigned to elemental S<sub>2s</sub>, S<sub>2p</sub> and Ca<sub>2p</sub> possibly caused by surface contamination. In addition to the contributions to the spectra from native cellulose, phosphorylated fibers show three new peaks at 134.4, 190.5 and 401.4 eV which can be assigned to P<sub>2p</sub>, P<sub>2s</sub><sup>34,35,37</sup> and N<sub>1s</sub><sup>36</sup> species. The appearance of elemental phosphorus peaks strongly supports the hypothesis that phosphorus moieties have been successfully incorporated in to the cellulose. The N<sub>1s</sub> species are most probably NH<sub>4</sub><sup>+</sup> groups of ammonium phosphate salt<sup>36</sup>, since the N<sub>1s</sub> peak due to surface contamination is probably washed

away in the same way as Ca and S, as shown in both Figures 4a and 4b where the Ca and S peaks have disappeared for the treated samples which have been exposed to extensive washing.

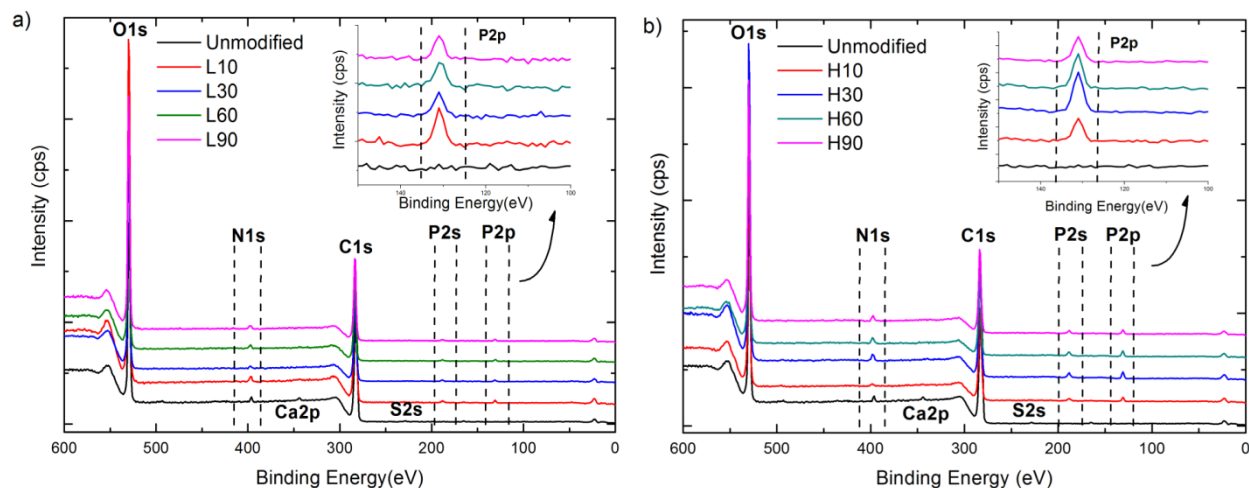
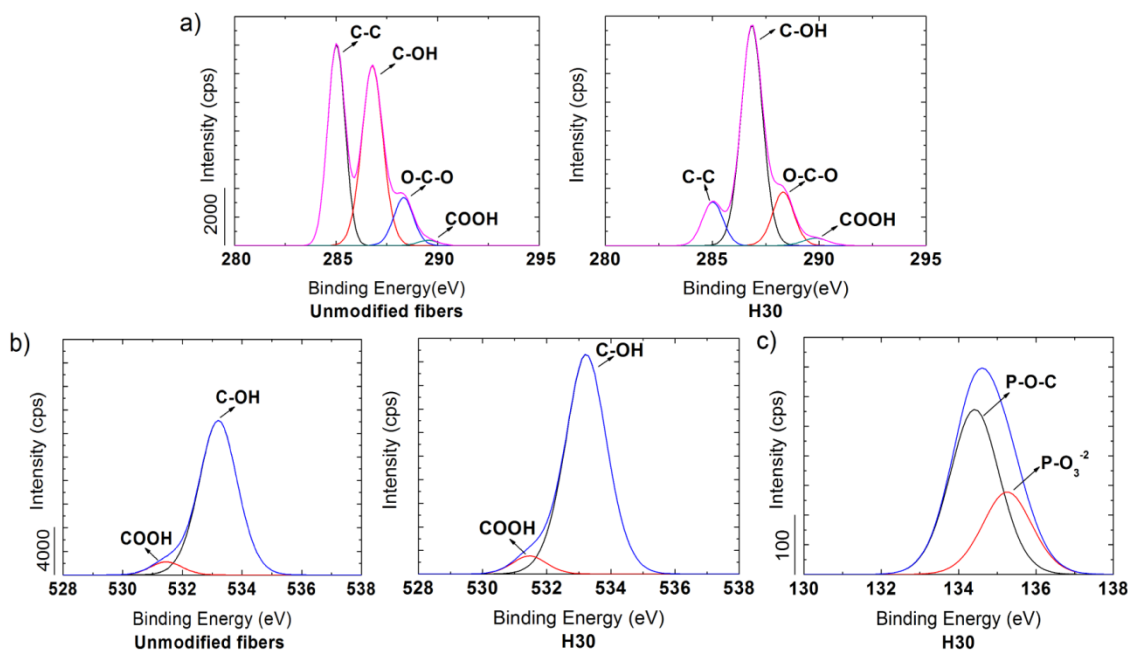


**Figure 4.** XPS spectra of unmodified and phosphorylated fibers: (a) Fibers phosphorylated at a low molar ratio of AGU:(NH<sub>4</sub>)<sub>2</sub>HPO<sub>4</sub>; (b) Fibers phosphorylated at a high molar ratio of AGU:(NH<sub>4</sub>)<sub>2</sub>HPO<sub>4</sub>

The relative surface concentrations of C, O and P atoms can be calculated in situ by integrating the areas under the peaks associated with each atom, see SI (Table S1). The P surface concentration increases when the fibers are modified at the two different molar ratios of AGU:(NH<sub>4</sub>)<sub>2</sub>HPO<sub>4</sub>, while the C surface concentration on fibers decreases. The highest C atomic percentage is on the unmodified fibers (70.4%) while H60 shows the lowest C atomic percentage (52.6%). The opposite effect was detected for surface concentration of O, where the atomic percentage increased from 29.6% on unmodified fibers to 43.8% on H60.

High resolution scan XPS spectra of C<sub>1s</sub>, O<sub>1s</sub> and P<sub>2p</sub> are shown in Figure 5a, 5b and 5c respectively for unmodified fibers and H30 with the highest P surface concentration. The C<sub>1s</sub> spectra are divided into four sub-peaks corresponding to different types of C-O bonds<sup>35,36</sup>. The

1 unmodified fibers display strong peaks at 285 and 286.8 eV attributed to C-C/C-H and C-OH  
 2 bonds respectively and two shoulder peaks at 288.2 and 289.6 eV attributed to O-C-O and O=C-  
 3 O bonds<sup>34-36</sup>. Compared to the unmodified sample, the intensity of the C-C bond is much lower  
 4 in phosphorylated fibers, and the shoulder peak at 289.6 eV assigned to O=C-O bonds  
 5 (carboxylate functionalities) seems to be larger in the phosphorylated fibers, possibly due to  
 6 partial oxidation. A decrease in intensity of the C-C bond in the phosphorylated fibers is  
 7 reasonable, since the outer surface of the modified fibers/fibrils is probably covered by  
 8 phosphate<sup>38</sup> and carboxylate functionalities.



10 **Figure 5.** XPS spectra of unmodified and phosphorylated fibers (H30); high resolution scans of:  
 11 (a) C<sub>1s</sub>; (b) O<sub>1s</sub> and (c) P<sub>2p</sub> (only modified fibers are shown for obvious reasons)

12 The O<sub>1s</sub> spectra of unmodified and phosphorylated fibers show a strong peak at 533.2 eV  
 13 assigned to C-OH bonds<sup>35,36</sup>, but the bands centered at 533.5 eV can also be assigned to C-O-P  
 14 groups<sup>36,37,39</sup>, and in the case of the phosphorylated fibers it seems that this peak is overlapped by

the peak associated with C-OH group. There is also a shoulder peak at 531.4 eV in both spectra assigned to P=O in phosphate and C=O groups<sup>35,36</sup> for which the intensity is greater in the phosphorylated fibers. The P<sub>2p</sub> spectra of phosphorylated fibers show non-resolved doublets corresponding to P<sub>2p1/2</sub> at 135.2eV and P<sub>2p3/2</sub> at 134.2eV<sup>35,36</sup>. The binding energies at 134 and 135eV are usually assigned to P-O-C or -PO<sub>3</sub><sup>-2</sup> groups when phosphate components react with cellulose<sup>36,37</sup>.

The bulk degree of substitution of phosphate groups (DS<sub>phosphate</sub>) is estimated from the ratio of the area under the P-O-C peak to the area under the C-OH peak in the XPS spectra. Due to the high concentrations of O=C-O bonds on phosphorylated fibers, the bulk DS of carboxylate groups (DS<sub>carboxylate</sub>) is also estimated by the same method, see SI (Table S2). In addition to the DS<sub>phosphate</sub> and DS<sub>carboxylate</sub>, the amount of charges introduced onto the fibers by each group, calculated on the basis of the DS values are also included in Table S2.

*3.1.4. <sup>13</sup>C CP/MAS NMR analysis.* The <sup>13</sup>C CP/MAS NMR spectra of unmodified fibers and L30, L90, H30 and H90 samples are shown in Figure 6. This study was carried out in order to estimate the impact of the phosphorylation on the supramolecular structure of cellulose I and possibly any region selectivity of the phosphorylation reaction. It is apparent from the spectra that an increase in the molar ratio of AGU:(NH<sub>4</sub>)<sub>2</sub>HPO<sub>4</sub> and in curing time leads to more extensive structural changes in the phosphorylated fibers. The assignment of different carbons of anhydroglucose units is also indicated in Figure 6, the region at 58-68 ppm is assigned to C6, the cluster of signals at 68-80 ppm to C2, C3 and C5, the region at 80-91 ppm to C4 and the region at 101-109 ppm to C1<sup>40</sup>.

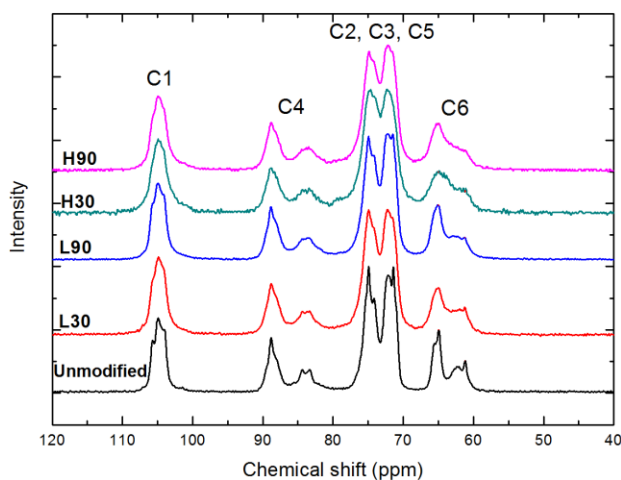


**Figure 6.**  $^{13}\text{C}$  CP/MAS NMR spectra of unmodified and phosphorylated fibers (L30, L90, H30 and H90)

As mentioned, a loss of spectral detail accompanied with the increased degree of phosphorylation, interpreted as a gradual loss of order of the cellulose, is the most pronounced tendency within the series<sup>30</sup>. This effect is specifically shown in H30 with the highest  $\text{DS}_{\text{phosphate}}$  of the tested samples. The sharper components of C4 and C6 regions assigned to the crystalline core of cellulose<sup>41</sup> tend to broaden from unmodified fibers to H30. Although spectral deterioration is most clearly observed in the C6 and C4 regions, phosphorylated fibers also show broader peaks in other regions. It is not therefore possible to determine any region selectivity of the phosphorylation reactions. Relative spectral change in the C4 and C1 regions which correspond to carbons of the glycosidic bond which are not available for substitution, indicates a possible modification in the neighboring atoms of C2 and C3<sup>21</sup>. The spectra recorded on the unmodified fibers were used for estimating the specific surface area of the water swollen cellulose I. The obtained surface-to-volume ratio and specific surface area were  $0.112 \pm 0.003$  and  $134 \pm 4 \text{ m}^2/\text{g}$  respectively, calculated from the NMR-estimates of the average lateral dimension of the cellulose I fibril aggregates<sup>31,32</sup>.

### 3.2. Morphological characterization of phosphorylated CNF.

Using the micro-fluidization process phosphorylated fibers were defibrillated by the shear forces producing a clear gel-like suspension of approx. 2 wt.%. Due to partial dissolution of fibers phosphorylated at the higher AGU:(NH<sub>4</sub>)<sub>2</sub>HPO<sub>4</sub> molar ratio, only fibers phosphorylated with a AGU:(NH<sub>4</sub>)<sub>2</sub>HPO<sub>4</sub> ratio of 1:1.2 were used to prepare CNF.

*3.2.1. AFM & cryo-TEM analysis of fibrils.* The phosphorylated fibrils prepared from L10, L30 and L60 denoted P-CNF10, P-CNF30 and P-CNF60 were imaged in solution using cryo-TEM and in the adsorbed state on dry surfaces using AFM, as shown in Figure 7. Individual fibrils are observed in all the samples while fibril aggregates increase in size and amount from P-CNF10 to P-CNF60. The width of the phosphorylated fibrils is estimated to be around 3 nm for all samples based on AFM images, as indicated in Table 4. On the other hand, the length of the phosphorylated fibrils shows a rather large variation. Although the length of the most of the fibrils is in the range of 500-1000 nm, there are fibrils with lengths less than 300 nm (especially in the case of P-CNF60) and over 1 μm.

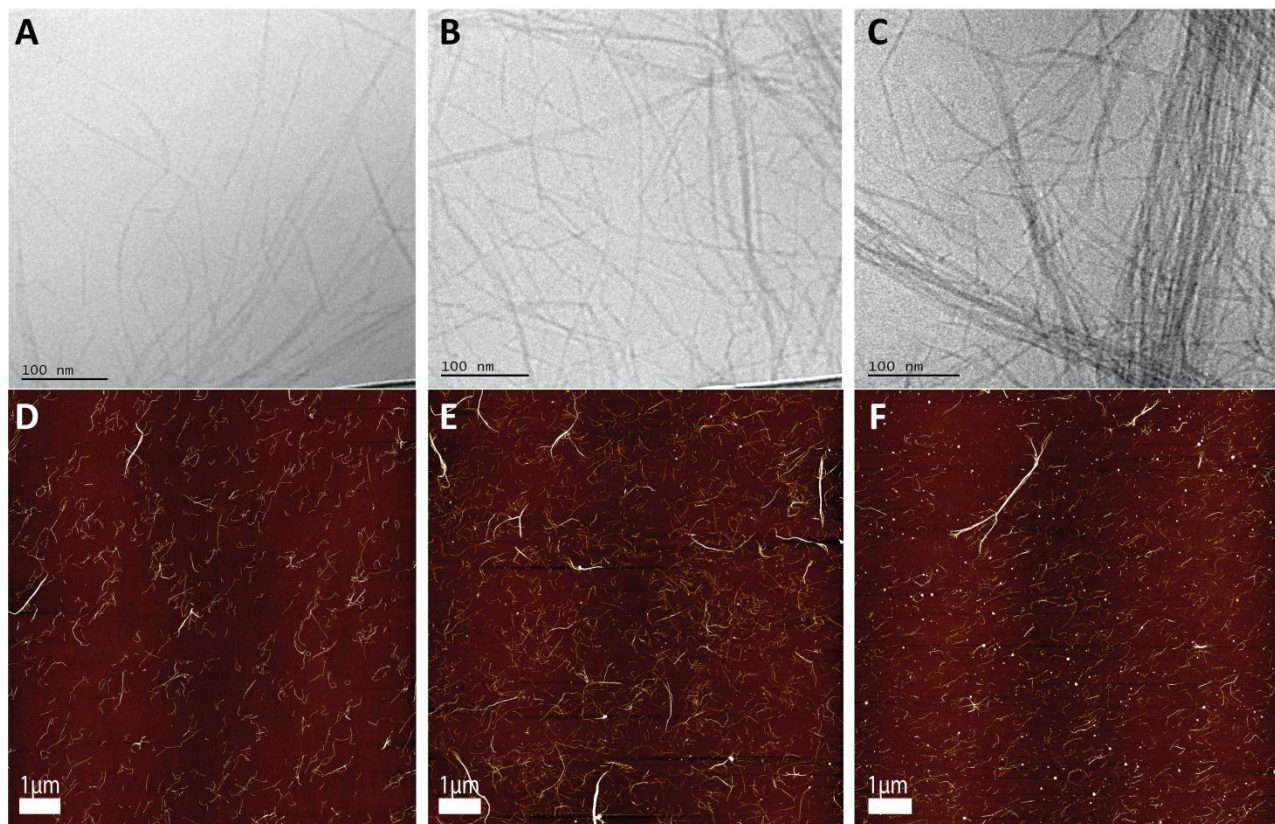


**Figure 7.** Images of: (A,D) P-CNF10; (B,E) P-CNF30 and (C,F) P-CNF60. (A-C) Fibrils in solution imaged with cryo-TEM and (D-F) fibrils adsorbed on silica surfaces imaged with AFM

The widths of phosphorylated fibrils were also measured based on cryo-TEM images, using a limited number of particles, as presented in Table 4. In agreement with the results of the AFM measurements, the width of the phosphorylated fibrils was independent of curing time and total charge of fibers, but it was not possible to evaluate an accurate length of fibrils from the cryo-TEM images, since individual fibrils often overlapped or ended in fibril aggregates in P-CNF dispersions. Larger fibril aggregates were observed particularly in P-CNF60, generally 20-100 nm wide and often over 10  $\mu\text{m}$  long, as measured by cryo-TEM.

**3.2.2. Determination of gravimetric yield.** The amount of stable CNF dispersion after homogenization and ultra-sonication, known as the gravimetric yield<sup>28,42</sup>, was measured for P-

CNF10, P-CNF30 and P-CNF60 after the stable CNF dispersion had been separated from aggregates and non-fibrillated fiber fragments by centrifugation<sup>42</sup>. The gravimetric yield of P-CNFs together with CNF prepared from enzymatically pretreated fibers, as evaluated by Fall et al.<sup>42</sup> are collected in SI (Table S3). The enzymatic CNF can be considered as a reference in this work, since it was prepared from fibers with the same chemical composition and since the enzymatic pretreatment contributes to fiber swelling<sup>18</sup> with no addition of ionic groups. It was possible to gain yields above 50% for P-CNF samples (as shown in Table S3), which is greater than with enzymatically prepared CNF.

### **3.3. Thermal stability and flame retardancy of phosphorylated CNF.**

The thermal stability and flame retardancy of phosphorylated CNF were studied for nanopaper sheets prepared from P-CNF10. Nanopaper sheets with a grammage of  $90.2 \pm 5.1$  (g/m<sup>2</sup>) and a thickness of  $65 \pm 6$  (μm) were used, named P-nanosheets hereafter.

*3.3.1. TGA analysis.* The thermal and thermo-oxidative stabilities of the P-nanosheets were assessed by thermogravimetric analysis in comparison with the properties of unmodified pulp fibers, as shown in Figure 8 (TG and dTG/dT curves in nitrogen and air).

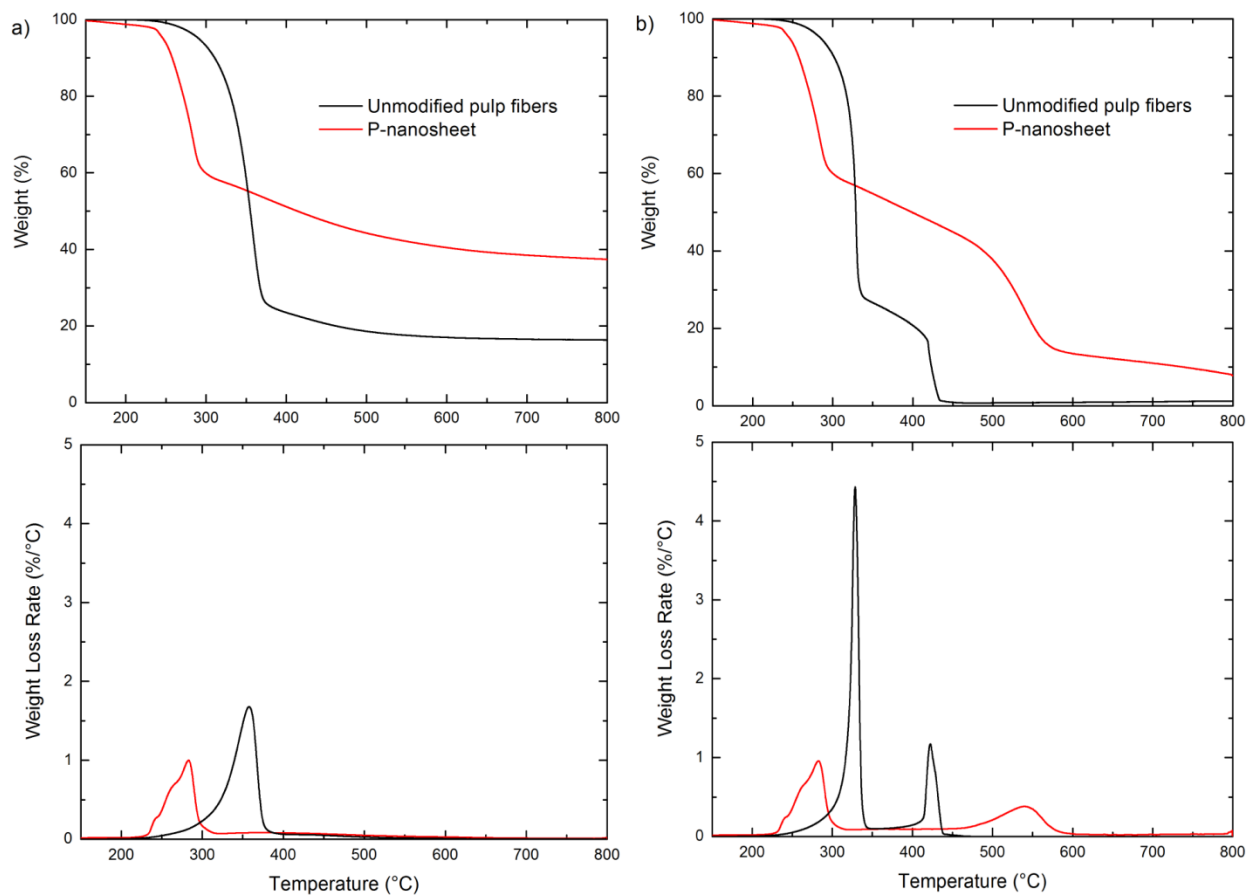


**Figure 8.** TG and dTG/dT curves of: (a) nanosheet of phosphorylated CNF (P-nanosheet) and unmodified pulp fibers in nitrogen; (b) P-nanosheet and unmodified pulp fibers in air

The thermal degradation of cellulose in nitrogen proceeds in a single step, during which the maximum weight loss occurs (Figure 8a). The pyrolysis of cellulose in nitrogen is usually defined by two pathways involving the decomposition of the glycosyl units to char at a lower temperature and the depolymerization of such units to volatile products at higher temperatures<sup>2,5,43</sup>. Compared to the unmodified pulp fibers, the presence of phosphorus in nanopaper sheet structure caused an earlier dehydration of cellulose toward char formation and a strong reduction in the cellulose decomposition temperature, as revealed by the  $T_{\text{onset10\%}}$  and  $T_{\text{max}}$

values (258°C vs 315°C and 283°C vs 358°C for the P-nanosheet and pulp fibers, respectively).

The final residue at the end of the test was 20% for pulp fibers and 40 % for P-nanosheet.

The thermo-oxidative stability was also investigated in air, where the dTG/dT curves show two decomposition peaks (Figure 8b), the first representing the creation of aliphatic char and volatile products, and the second the conversion of aliphatic to aromatic char and the release of CO and CO<sub>2</sub> as a result of the simultaneous carbonization and char formation<sup>2,5,43</sup>. As in nitrogen, the presence of phosphorus induced an earlier cellulose dehydration and lower maximum weight loss temperatures ( $T_{\text{onset}10\%}$  and  $T_{\text{max}1}$  respectively) than unmodified pulp fibers. Compared to the pulp fibers, the char formed during the first degradation step of the P-nanosheet was thermally more stable, as indicated by the  $T_{\text{max}2}$  values (539°C for P-nanosheet vs 422°C for pulp fibers), leaving a significantly greater residue from the nanopaper sheet at 800°C.

*3.3.2. Flammability & Cone Calorimeter testing.* In order to investigate the behavior of phosphorylated CNF at early stages of burning, P-nanosheets were subjected to both flammability and forced combustion tests. These two tests together provide complementary information concerning the flame-retardant properties of the phosphorylated CNF.

The reaction of the P-nanosheet to direct flame exposure was studied in comparison with that of a filter paper of the same thickness through the flame spread test. It is important to test the sample behavior on exposure to a flame, in order to evaluate the propensity of the material to initiate fire. For this reason, both the P-nanosheet and the filter paper were subjected to a flammability test in horizontal configuration. Figure 9 presents snapshots taken at fixed times during the tests on the papers. When the flame was applied, the filter paper immediately ignited and burned with a flame which lasted throughout the test leaving 0% residue. In contrast, once the flame was applied to

the P-nanosheet, it burned very slowly and it self-extinguished as soon as the flame was removed from the sample. Even after a second and third application of the flame, the P-nanosheet was able to stop the flame spreading and self-extinguished. Compared to the filter paper, a strong reduction in the burning rate (-33%) and a consistent final residue of 92% was found with the P-nanosheet.

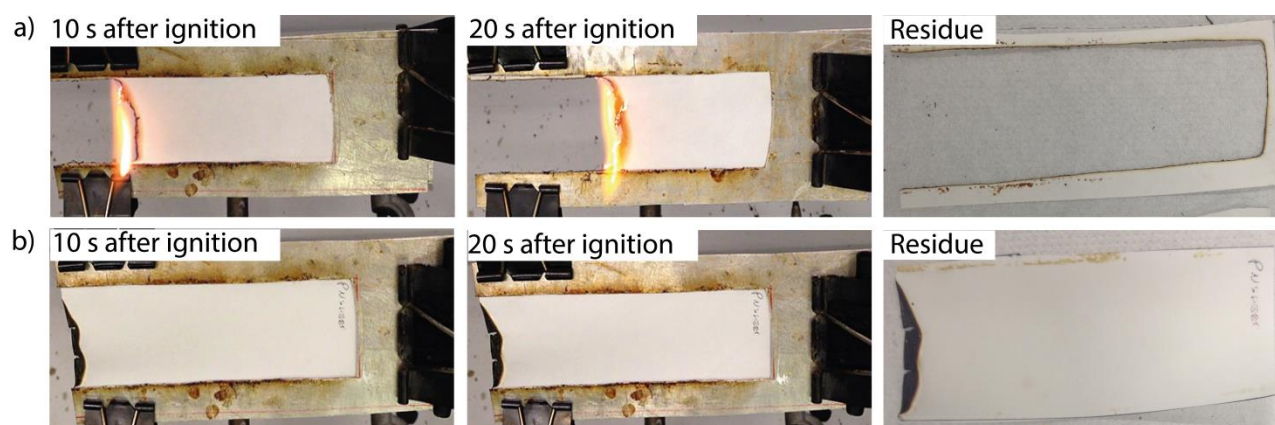


**Figure 9.** Snapshots of: (a) filter paper; (b) P-nanosheet taken at fixed times during the flammability test

The resistance of the P-nanosheet to an irradiative heat flux of  $35\text{kW/m}^2$  was compared to that of the filter paper through cone calorimetry tests. The exposure to the cone heat flux ( $35\text{kW/m}^2$ , typical of early developing fires) leads to a sudden increase in the surface temperature of the sample (up to  $400\text{-}500^\circ\text{C}$ ); and as a consequence the sample undergoes thermal degradation with the release of combustible volatile species that led to the ignition (TTI) in the case of the filter paper and subsequent flaming combustion (pkHRR and THR). Figure 10 shows the HRR plots for the filter paper and the P-nanosheet as a function of time. The filter paper yielded an average TTI of 44 s with pkHRR of  $42.7\text{ kW/m}^2$  and THR of  $0.7\text{ MJ/m}^2$ . Surprisingly, the nanopaper sheet exhibited no ignition at all under the cone calorimeter, preserving more than twice as much

material after the test compared to the filter paper. This behavior is quite unusual for a cellulosic material which normally burns quickly when it is exposed to the cone calorimetry heat flux. Cone calorimeter data (Table S6) and images of the filter paper and the P-nanosheet before and after cone calorimetry (Figure S1) are provided in SI.

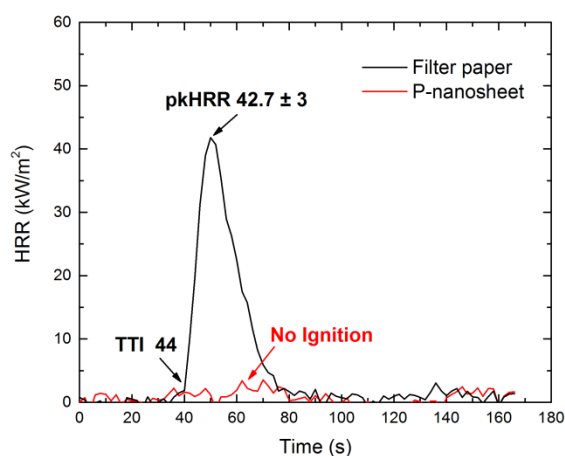


**Figure 10.** Results from cone calorimetry tests showing HRR curves: black line: filter paper; red line: P-nanosheet

### 3.4. Mechanical properties of nanopaper sheets.

The mechanical properties of the P-nanosheets were determined and compared with earlier reported values<sup>44</sup>. In earlier work, Henriksson et al.<sup>44</sup> used enzymatically treated softwood dissolving pulps with different degrees of polymerization (DP) of the constituent cellulose. The DP of the phosphorylated CNF is calculated from intrinsic viscosity data,  $\eta$  where  $\eta = 0.42DP$  for  $DP < 950$  and  $\eta = 2.28DP^{0.76}$  for  $DP > 950$ <sup>28,44</sup>. The viscosity measurement was performed at MoRe Research AB (Örnsköldsvik, Sweden) where the CNF samples were dissolved in a copper ethylenediamine solution (ISO-5351). The samples were never allowed to completely dry before dissolution which is a derivation from the standard viscosity measurement<sup>28</sup>. The DP of the

fibrils, film density as well as specific strength and specific modulus (normalized values) of P-nanosheet and nanopapers from the earlier work are presented in the SI (Table S4)<sup>28,44</sup>. It is shown by Henriksson et al. that an increase in DP is followed by an increase in the strength of the nanopapers. DP-580 (Henriksson et al.) was prepared from fibrils with the closest DP to the phosphorylated fibrils of the present work. In comparison, the P-nanosheet has a relatively good specific strength ( $1.49 \text{ (Nm/kg)} \cdot 10^{-5}$  vs  $1.39 \text{ (Nm/kg)} \cdot 10^{-5}$  for P-nanosheet and DP-580, respectively) and shows an even higher strain at break (7.5% vs 6.4% for P-nanosheet and DP-580 respectively). In contrast the specific modulus is lower in the P-nanosheet ( $6.11 \text{ (Nm/kg)} \cdot 10^{-6}$  vs  $9.39 \text{ (Nm/kg)} \cdot 10^{-6}$ ), representing a film with lower stiffness<sup>28</sup>. The strain rate applied in the present work was lower than that applied in the work of Henriksson et al.<sup>44</sup> which can also lead to a lower modulus.

## **4. Discussion**

### **4.1. Chemical structure of the phosphorylated fibers/fibrils.**

Pulp fibers were successfully phosphorylated using  $(\text{NH}_4)_2\text{HPO}_4$  and urea as reagents as was shown by conductometric titration, FT-IR and XPS analysis. A large increase was generally observed in the total fiber charge upon phosphorylation, which is a sign of attachment of phosphate groups and which was increased using a higher molar ratio of AGU: $(\text{NH}_4)_2\text{HPO}_4$ :Urea and a longer curing time. The results of the total charge measurement indicate that it is not possible to reach charges higher than 1.84 meq./g by increasing the curing time, probably because of cellulose dissolution due to the high DS values reached at this high charge. Other consequences of a higher charge are an increased swelling of the fibers and an easier delamination of the fiber wall during subsequent homogenization<sup>14</sup>. The dissolution of the

cellulose at higher DS is also increased in the presence of urea, which is known to be a solvent aid for cellulose<sup>45-47</sup>.

Results of FT-IR spectroscopy showed the average chemical structure of the phosphorylated fibers and the chemical composition and structure of the fiber surface were shown by XPS. The appearance of P=O and P-OH bonds provided support for the phosphorylation and the absence of P-H bond adsorption ( $2280-2440\text{ cm}^{-1}$ <sup>27,34</sup>) in the FT-IR spectra of the modified fibers suggests that most of the phosphorus is attached to cellulose in the form of phosphate groups containing two acidic protons. The same results were obtained in the XPS study where the appearance of bands centered at 134.5eV shows that phosphorus exists in its pentavalent state in the form of C-O-P(=O)(O)<sub>2</sub><sup>-</sup> on modified fibers<sup>37</sup>. The decrease in the atomic percentage of carbon and increase in the atomic percentage of oxygen with increasing AGU:(NH<sub>4</sub>)<sub>2</sub>HPO<sub>4</sub>:Urea molar ratio and curing time, as shown in Table 2, are also in agreement with surface phosphorylation. For each grafted phosphate group, one free hydroxyl group is substituted by two new hydroxyl groups and one phosphoryl group, and this leads to an increase in the atomic concentration of oxygen<sup>48</sup>. The decrease in the atomic percentage of P in L90 and H90 is also in agreement with the results of the conductometric titration where longer curing times led to a lower total charge of the fibers.

FT-IR and XPS studies also show that partial oxidation occurs on the fibers during phosphorylation. The appearance of a sharp carbonyl peak in the FT-IR spectra and an increase in intensity of the O=C-O band in high resolution XPS spectra of phosphorylated fibers compared to unmodified fibers show the creation of carboxylate functionalities in addition to phosphate attachment on the cellulose. In an oxygen-rich atmosphere at 150°C, oxidation of functional groups of cellulose is assumed to progress slowly with a variety of transitional products<sup>49</sup>, and partial oxidation of the fibers is expected to occur, considering the phosphorylation reaction

conditions. The O=C-O band is also observed in high-resolution XPS spectra of unmodified fibers, as shown in Figure 5b. But, compared to phosphorylated fibers the intensity is significantly lower and can be explained by a low hemicellulose content of unmodified fibers. These hemicelluloses are probably removed during the phosphorylation reaction.

According to Table 3, the total charge of unmodified and phosphorylated fibers is the sum of charges associated with phosphate and carboxylate functionalities, as determined by XPS and also demonstrated by the conductometric titration. The discrepancy in absolute values between these methods can be traced back to the complexity of evaluating the degree of substitution with these methods. In the conductometric titration both monobasic (carboxylate groups) and dibasic (phosphate groups) acids are contributing to the total charge and it is very difficult, if not impossible, to separate the different groups with only the titration since the groups have average  $pK_a$  values not too far apart, especially for these types of polyelectrolytic surfaces. The XPS study, on the other hand, specifically measures the phosphorus content even though the intensity integration is not an exact method either to determine the absolute concentration of the phosphorus in the fibers. But, due to the specificity of the XPS for phosphorus this method was chosen over conductometric titration for the determination of the bulk  $DS_{\text{phosphate}}$ .

#### **4.2. Estimation of the surface substitution of phosphate groups of the fibrils.**

When discussing the location of the phosphate groups in the fiber wall, it is important to remember the hierarchical structure of the cellulose fibers. In the delignified fiber wall, the average lateral fibril dimensions are approximately 4x4 nm, and fibrils are aggregated into fibril aggregates with an average lateral dimension of about 20x20 nm<sup>32</sup> and it has recently been found that, even at high levels of substitution, these aggregates are kept together so that the interior of

the aggregates is inaccessible to the chemical reagents<sup>31</sup>. This means that the phosphorylation of the fiber wall is primarily a surface modification of the fibril aggregates.

In order to calculate the surface  $DS_{\text{phosphate}}$ , the fraction of AGU accessible for modification (surface-to-volume ratio,  $q$ ) must be taken into account. Assuming a simple model for fibril aggregates where they have a square cross-section, the average surface-to-volume ratio of the fibril aggregates can be determined from signal intensities of the C4 region of the  $^{13}\text{C}$  CP/MAS NMR spectra of cellulose<sup>30,31</sup>. The surface  $DS_{\text{phosphate}}$  of the cellulose fibril aggregate can be estimated by dividing the bulk  $DS_{\text{phosphate}}$  by the so obtained  $q$  value. For the phosphorylated fibers examined by  $^{13}\text{C}$  CP/MAS NMR, the relative surface  $DS_{\text{phosphate}}$  based on  $q$  value of unmodified fibers are given in SI (Table S5). The reason for this approximation is that it was not possible to determine  $q$  values of H30 and H90 due to extensive broadening of the C4 region in  $^{13}\text{C}$  CP/MAS NMR spectra. If the supramolecular structure of cellulose I during the phosphorylation is similar to the supramolecular structure in the water swollen state, this approximation will not introduce any significant error.

The surface  $DS_{\text{phosphate}}$  on the fibril aggregates of unmodified fibers, L30, L90, H30 and H90 together with the total charge of fibers and bulk  $DS_{\text{phosphate}}$  calculated previously from XPS are listed in Table S5. As expected,  $DS_{\text{phosphate}}$  is higher for the fibril aggregate surface than the bulk  $DS_{\text{phosphate}}$  as determined from XPS measurements<sup>32</sup>. Even with a large total charge (1.84 meq./g for H30), the surface  $DS_{\text{phosphate}}$  did not exceed 0.5. This suggests that even at very high levels of modification not more than one hydroxyl group per surface anhydroglucose unit was phosphorylated which could be a sign of some region-selectivity of the phosphorylation reaction, as shown by Bozic et al.<sup>34</sup>, Wanrosli et al.<sup>50</sup> and Granja et al.<sup>21</sup>. Among available reaction sites, the probability of phosphorylation on C6 hydroxyl groups is highest, since this group is least

sterically hindered of all the available hydroxyl groups in the glucose moiety<sup>50</sup>. A surface  $DS_{\text{phosphate}}$  of 0.41 obtained for H30 thus corresponds to selective phosphorylation of the C6 groups at the surface of their fibril aggregates. It is hence important to note that despite a low average concentration of the phosphate in the fiber material there is a rather high surface substitution of the phosphate groups on the fibrils. This will naturally be very important when trying to understand the properties of the modified fibrils.

#### **4.3. The effect of chemical reaction conditions on the fibrillation of fibers.**

The measured gravimetric yield shows the extent of fibrillation for the enzymatically treated and for the phosphorylated fibers. It has previously been shown that charge density of pulp fibers is one of the properties most affecting the fibrillation process<sup>28,42</sup>. It is well known that an increase in charge leads to a higher osmotic pressure inside the fiber wall and hence a higher fiber swelling and this in turn leads to a more efficient liberation of the fibrils during homogenization<sup>14</sup>. It has also been shown that, once liberated, the fibrils with a higher charge will have a greater stability against aggregation<sup>14,42</sup>. P-CNF30 prepared from fibers with higher charge density had a greater gravimetric yield than P-CNF10. But the same trend was not followed for P-CNF60, for which the pulp fibers contained an even greater number of charges, which indicates that other factors than the charge are of importance for the efficiency of the fibrillation process.

Cryo-TEM images of P-CNF dispersions (Figure 11) show less individual fibrils, especially for P-CNF60 for which a lower gravimetric yield is expected. While fibril aggregates are loosened up for P-CNF10 and P-CNF30 dispersions, they are in a more aggregated state for P-CNF60

showing that fibrillation has not occurred evenly throughout the fibers. One possible reason for this is that despite of high charge density; P-CNF60 is prepared from fibers which were exposed to high temperature oven curing for a longer time than the other two samples. When cellulose substrates are dried from water under severe conditions, hornification occurs. This phenomenon, which is an irreversible closure of fiber wall pores, results from the removal of water and the formation of new intermolecular links between cellulose fibrils<sup>32</sup>. Fibers cured for a longer time at 150°C also have their fiber wall collapsed to a greater extent. Therefore once wetted, they cannot re-swell to the same degree and this leads to a stiffer fiber wall which is not easily opened during the homogenization process.

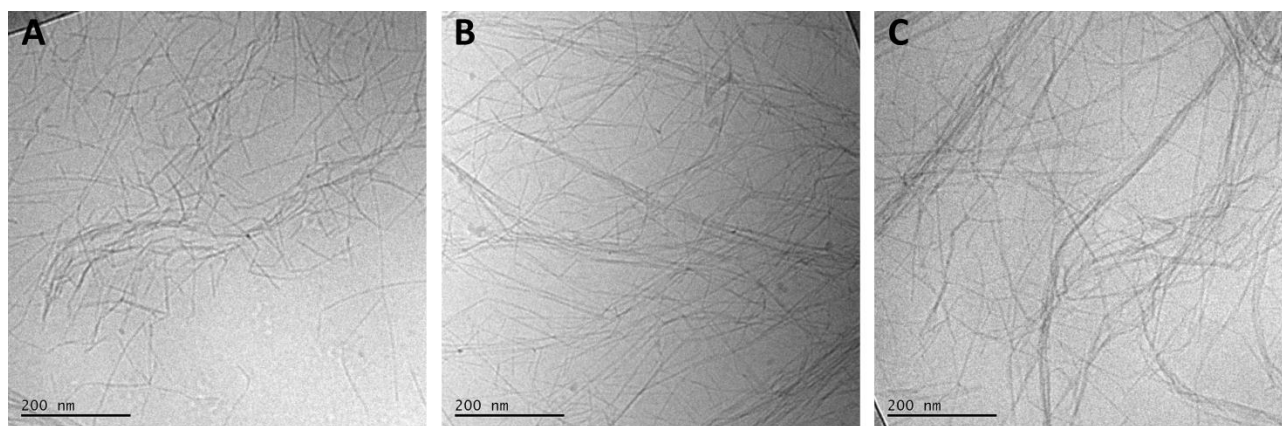


**Figure 11.** Cryo-TEM images of phosphorylated CNF dispersion: (A) P-CNF10 dispersion; (B) P-CNF30 dispersion; (C) P-CNF60 dispersion

#### 4.4. Thermal stability and Flame-retardant performances.

The enhanced thermal and flame- retardant performances of phosphorylated CNF presented in the form of nanopaper sheet, compared to unmodified fibers and normal filter paper can be explained by the presence of a high concentration of phosphate groups on the surface of the fibrils which catalyze the dehydration and prevent thermal decomposition of cellulose<sup>5,43</sup>. As a

consequence of the temperature increase, the cellulose undergoes pyrolysis as a result of which heterolytic bond scission along the molecular chain occurs. This leads to the generation of levoglucosan, a volatile monomer which is a 1,6-anhydro ring formed by glucose. The instability of the cellulose C6 hydroxyl group then plays a crucial role in cellulose depolymerization<sup>51</sup>. If phosphorylation of fibers mainly occurs on C6 hydroxyl groups, the main depolymerization mechanism of CNF is blocked. Furthermore, compared to unmodified fibers, the earlier thermal and thermo-oxidative degradation of phosphorylated fibrils is also attributed to the release of phosphoric acid which catalyzes the dehydration of cellulose to form an aromatic carbonaceous structure such as char<sup>2,5</sup>.

All this means that when subjected to a flame or a heat flux the P-nanosheet can hence rapidly form a thermally stable char, inhibiting production of volatile components and protecting the uncombusted material from direct flame contact, thus resulting in a self-extinguishing behavior during flammability tests and preventing ignition during cone calorimetry. This also means that by grafting 0.85 % (w/w) phosphate groups to fibers; they are converted to a flame-retardant material.

#### **4.5. Mechanical performance.**

The specific strength and strain at break of nanopaper sheets prepared from phosphorylated CNF are comparable to those of earlier reported nanopapers with outstanding mechanical properties<sup>44</sup>. This is naturally important since the flame-retardant materials also need to have a mechanical integrity when applied in more complex material concepts. In this respect the liberation of the fibrils from fibril aggregates into free fibrils is important since a higher number concentration of the fibrils will lead to a higher number of fibril contacts in the prepared nanopaper. The

phosphorylated fibrils used to prepare nanopaper sheets have a high surface DS of phosphate and carboxyl groups and this will lead to a lower ordering of the molecules on the surface of the fibrils allowing for a more efficient contact between the fibrils in the dry nanopaper and hence a stronger nanopaper sheet. On the other hand, the existence of fibril aggregates and fewer free fibrils, as in the case of P-CNF10, has a negative effect on the number of fibril/fibril contacts and a less efficient contact between the fibrils which could be the reason for the lower stiffness of the P-CNF10 nanopaper<sup>28</sup>. The most important finding is however that the flame-retardant nanopaper also has very good mechanical properties compared to other types of nanopapers from CNF.

## 5. Conclusions

A controlled phosphorylation of pulp fibers containing mainly cellulose was achieved using  $(\text{NH}_4)_2\text{HPO}_4$  in the presence of urea, as shown by FT-IR, XPS and solid state NMR spectroscopy. Upon phosphorylation, the fibers become highly charged due to the attachment of phosphate and carboxylate functionalities, and this makes phosphorylation a suitable chemical pre-treatment for the preparation of phosphorylated CNF through a homogenization process. With this technique it was possible to prepare phosphorylated fibers with different degrees of substitution with phosphate and carboxylate groups (bulk  $\text{DS}_{\text{phosphate}}$  from 0.014 to 0.047 and  $\text{DS}_{\text{carboxylate}}$  from 0.024 to 0.05). By using the results obtained from  $^{13}\text{C}$  CP/MAS NMR spectra in combination with the results from XPS study the degree of substitution of polymers located at the surface of fibril aggregates (surface  $\text{DS}_{\text{phosphate}}$ ) could be determined. The maximum surface  $\text{DS}_{\text{phosphate}}$  obtained was 0.41 which suggests that phosphorylation occurs mainly at the surface of fibril aggregates and a high surface DS can hence be achieved at a still very moderate bulk modification of the cellulose.

For the first time, to the knowledge of the authors, cellulose nanofibrils were prepared from the phosphorylated fibers using no other pretreatment, yielding fibrils with widths of approximately 3 nm and lengths between 500 and 1000 nm. The CNF dispersions prepared from different phosphorylated fibers have been shown to contain more than 50% colloiddally stable nanofibrils. Different reaction conditions affect fibrillation in a significant way and curing times (at 150°C) of less than 1 hour lead to a more efficient fibrillation during the homogenization process. It was also shown that the thermal stability and flame-retardant properties of nanopaper sheets prepared from phosphorylated CNF were largely improved compared to unmodified pulp fibers and filter paper. The nanopaper sheets showed a self-extinguishing behavior during flammability tests and did not ignite when subjected to the cone calorimeter heat flux despite have a substitution by weight as low as 0.85%. It was also shown that the mechanical properties of the modified fibrils are indeed comparable to earlier published data for CNF-based nanopapers. These findings are of great importance and clearly indicate that phosphorylated CNF represents an intrinsic cellulose-based flame-retardant material. While the nanopaper sheet presented in this work is the proof of concept, the material in the form of fibrils has a potential for use in more sustainable and comparatively environment friendly flame-retardant composites and nano coatings which are for instance made through layer by layer technique.

#### **Author information**

#### **Corresponding authors**

\*Email: [marygp@kth.se](mailto:marygp@kth.se)

\*Email: [wagberg@kth.se](mailto:wagberg@kth.se)

#### **Author contribution**

The manuscript was written through contribution of all authors. All authors have given approval to the final version of the manuscript.

### Notes

The authors declare no competing financial interest.

### Acknowledgment

Swedish Foundation for Strategic Research (SSF) is gratefully acknowledged for financial support and Lars Wågberg acknowledges Wallenberg Wood Science Centre (WWSC) for financial support. The authors would also like to thank MSc Kent Malmgren at SCA Research AB, Sundsvall, Sweden for excellent discussions and support during the development of the experimental procedure for the phosphorylation reactions.

### Associated content

### Supporting information

Surface concentration of C, O and P elements and values of bulk and surface  $DS_{\text{phosphate}}$  and  $DS_{\text{carboxylate}}$  on unmodified and phosphorylated fibers, values of gravimetric yield of enzymatic and phosphorylated CNF, mechanical properties of P-nanosheet, cone calorimeter data of the filter paper and P-nanosheet as well as pictures of the residues before and after cone calorimeter test. This material is available free of charge via the Internet at <http://pubs.acs.org>.

### References

- (1) Alongi, J.; Carosio, F.; Malucelli, G. *Polym. Degrad. Stab.* **2012**, *97*, 1644–1653.
- (2) Alongi, J.; Carletto, R. A.; Di Blasio, A.; Carosio, F.; Bosco, F.; Malucelli, G. *J. Mater. Chem. A* **2013**, *1*, 4779–4785.

- 1 (3) Horrocks, A. R.; Price, D. *Advances in Fire Retardant Materials*; CRC Press LLC:  
2 Cambridge, 2009.
- 3 (4) Cain, A. A.; Nolen, C. R.; Li, Y. C.; Davis, R.; Grunlan, J. C. *Polym. Degrad. Stab.* **2013**,  
4 98, 2645–2652.
- 5 (5) Alongi, J.; Carletto, R. A.; Bosco, F.; Carosio, F.; Di Blasio, A.; Cuttica, F.; Antonucci,  
6 V.; Giordano, M.; Malucelli, G. *Polym. Degrad. Stab.* **2014**, 99, 111–117.
- 7 (6) Camino, G.; Costa, L.; Luda di Cortemiglia, M. P. *Polym. Degrad. Stab.* **1991**, 33, 131–  
8 154.
- 9 (7) Alongi, J.; Di Blasio, A.; Cuttica, F.; Carosio, F.; Malucelli, G. *Eur. Polym. J.* **2014**, 51,  
10 112–119.
- 11 (8) Karabulut, E.; Pettersson, T.; Ankerfors, M.; Wågberg, L. *ACS Nano* **2012**, 6, 4731–4739.
- 12 (9) Karabulut, E.; Wågberg, L. *Soft Matter* **2011**, 7, 3467–3474.
- 13 (10) Sehaqui, H.; Liu, A.; Zhou, Q.; Berglund, L. A. *Biomacromolecules* **2010**, 11, 2195–2198.
- 14 (11) Hamed, M.; Karabulut, E.; Marais, A.; Herland, A.; Nyström, G.; Wågberg, L. *Angew.*  
15 *Chem. Int. Ed. Engl.* **2013**, 52, 12038–12042.
- 16 (12) Pääkkö, M.; Vapaavuori, J.; Silvennoinen, R.; Kosonen, H.; Ankerfors, M.; Lindström, T.;  
17 Berglund, L. A.; Ikkala, O. *Soft Matter* **2008**, 4, 2492.
- 18 (13) Turbak, A. F.; Snyder, F. W.; Sandberg, K. R. *J. Appl. Polym. Sci. Symp.* **1983**, 37, 815–  
19 827.
- 20 (14) Klemm, D.; Kramer, F.; Moritz, S.; Lindström, T.; Ankerfors, M.; Gray, D.; Dorris, A.  
21 *Angew. Chem. Int. Ed. Engl.* **2011**, 50, 5438–5466.
- 22 (15) Saito, T.; Nishiyama, Y.; Putaux, J. L.; Vignon, M.; Isogai, A. *Biomacromolecules* **2006**,  
23 7, 1687–1691.
- 24 (16) Pääkkö, M.; Ankerfors, M.; Kosonen, H.; Nykänen, A.; Ahola, S.; Osterberg, M.;  
25 Ruokolainen, J.; Laine, J.; Larsson, P. T.; Ikkala, O.; Lindström, T. *Biomacromolecules*  
26 **2007**, 8, 1934–1941.
- 27 (17) Wågberg, L.; Winter, L.; Ödeberg, L.; Lindström, T. *Colloids and Surfaces* **1987**, 27, 163–  
28 173.
- 29 (18) Henriksson, M.; Henriksson, G.; Berglund, L. A.; Lindström, T. *Eur. Polym. J.* **2007**, 43,  
30 3434–3441.

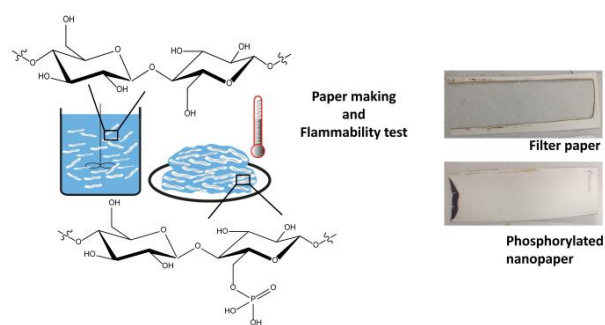
- 1 (19) Wågberg, L.; Decher, G.; Norgren, M.; Lindström, T.; Ankerfors, M.; Axnäs, K. *Langmuir*  
2 **2008**, *24*, 784–795.
- 3 (20) Reid, J. D.; Mazzeno, L. W. *Ind. Eng. Chem.* **1949**, *41*, 2828–2831.
- 4 (21) Granja, P. L.; Pouységu, L.; Pétraud, M.; De Jéso, B.; Baquey, C.; Barbosa, M. a. *J. Appl.*  
5 *Polym. Sci.* **2001**, *82*, 3341–3353.
- 6 (22) Inagaki, N.; Nakamura, S.; Asai, H.; Katsuura, K. *J. Appl. Polym. Sci.* **1976**, *20*, 2829–  
7 2836.
- 8 (23) Heinze, U.; Klemm, D.; Unger, E.; Pieschel, F. *Starch/Stärke* **2003**, *55*, 55–60.
- 9 (24) Coleman, R. J.; Lawrie, G.; Lambert, L. K.; Whittaker, M.; Jack, K. S.; Grøndahl, L.  
10 *Biomacromolecules* **2011**, *12*, 889–897.
- 11 (25) Nuessle, A. C.; Ford, F. M.; Hall, W. P.; Lippert, A. L. *Text. Res. J.* **1956**, *26*, 32–39.
- 12 (26) Aoki, D.; Nishio, Y. *Cellulose* **2010**, *17*, 963–976.
- 13 (27) Suflet, D. M.; Chitanu, G. C.; Popa, V. I. *React. Funct. Polym.* **2006**, *66*, 1240–1249.
- 14 (28) Fall, A. B.; Burman, A.; Wågberg, L. *Nord. Pulp Pap. Res. J.* **2014**, *29*, 176–184.
- 15 (29) Newman, R. H. *ACS Symp. Ser.* **1992**, *489*, 311–319.
- 16 (30) Larsson, P. T.; Wickholm, K.; Iversen, T. *Carbohydr. Res.* **1997**, *302*, 19–25.
- 17 (31) Wickholm, K.; Larsson, P. T.; Iversen, T. *Carbohydr. Res.* **1998**, *312*, 123–129.
- 18 (32) Chunilall, V.; Bush, T.; Larsson, P. T.; Iversen, T.; Kindness, A. *Holzforschung* **2010**, *64*,  
19 693–698.
- 20 (33) Tata, J.; Alongi, J.; Carosio, F.; Frache, A. *Fire Mater.* **2011**, *35*, 397–409.
- 21 (34) Božič, M.; Liu, P.; Mathew, A. P.; Kokol, V. *Cellulose* **2014**, *21*, 2713–2726.
- 22 (35) Viornery, C.; Chevolot, Y.; Léonard, D.; Aronsson, O. a; Péchy, P.; Mathieu, H. J.;  
23 Descouts, P.; Grätzel, M. *Langmuir* **2002**, *18*, 2582–2589.
- 24 (36) Bourbigot, S.; Le Bras, M.; Gengembre, L.; Delobel, R. *Appl. Surf. Sci.* **1994**, *81*, 299–  
25 307.
- 26 (37) Pasqui, D.; Rossi, A.; Di Cintio, F.; Barbucci, R. *Biomacromolecules* **2007**, *8*, 3965–3972.
- 27 (38) Li, K.; Wang, J.; Liu, X.; Xiong, X.; Liu, H. *Carbohydr. Polym.* **2012**, *90*, 1573–1581.

- (39) Cini, N.; Ball, V. *Adv. Colloid Interface Sci.* **2014**, *209*, 84–97.
- (40) Halonen, H.; Larsson, P. T.; Iversen, T. *Cellulose* **2012**, *20*, 57–65.
- (41) Rajaji, H. . A.; VanderHart, D. L. *Science (80-. )*. **1984**, *223*, 283–285.
- (42) Fall, A. B.; Lindström, S. B.; Sundman, O.; Ödberg, L.; Wågberg, L. *Langmuir* **2011**, *27*, 11332–11338.
- (43) Carosio, F.; Di Blasio, A.; Cuttica, F.; Alongi, J.; Malucelli, G. *Ind. Eng. Chem. Res.* **2014**, *53*, 3917–3923.
- (44) Henriksson, M.; Berglund, L. A.; Isaksson, P.; Lindström, T.; Nishino, T. *Biomacromolecules* **2008**, *9*, 1579–1585.
- (45) Qi, H.; Cai, J.; Zhang, L.; Kuga, S. *Biomacromolecules* **2009**, *10*, 1597–1602.
- (46) Chen, X.; Burger, C.; Wan, F.; Zhang, J.; Rong, L.; Hsiao, B. S.; Chu, B.; Cai, J.; Zhang, L. *Biomacromolecules* **2007**, *8*, 1918–1926.
- (47) Yang, Q.; Fukuzumi, H.; Saito, T.; Isogai, A.; Zhang, L. *Biomacromolecules* **2011**, *12*, 2766–2771.
- (48) Granja, P. L.; Pouységu, L.; Deffieux, D.; Daudé, G.; De Jéso, B.; Labrugère, C.; Baquey, C.; Barbosa, M. A. *J. Appl. Polym. Sci.* **2001**, *82*, 3354–3365.
- (49) Łojewska, J.; Miśkowiec, P.; Łojewski, T.; Proniewicz, L. M. *Polym. Degrad. Stab.* **2005**, *88*, 512–520.
- (50) Wanrosli, W. D.; Rohaizu, R.; Ghazali, a. *Carbohydr. Polym.* **2011**, *84*, 262–267.
- (51) Lecoeur, E.; Vroman, I.; Bourbigot, S.; Lam, T. M.; Delobel, R. *Polym. Degrad. Stab.* **2001**, *74*, 487–492.

1 **For Table of Contents Use Only**

2 Phosphorylated cellulose nanofibrils: A renewable nanomaterial for the preparation of  
3 intrinsically flame-retardant materials

4 Maryam Ghanadpour, Federico Carosio, Per Tomas Larsson and Lars Wågberg



5